

# Linear coupling of modes in 2D radially stratified astrophysical discs

A. G. Tevzadze<sup>1</sup>, G. D. Chagelishvili<sup>1,2</sup>, G. Bodo<sup>3</sup> and P. Rossi<sup>3</sup>

<sup>1</sup> *Georgian National Astrophysical Observatory, Chavchavadze State University, Tbilisi, Georgia*

<sup>2</sup> *Nodia Institute of Geophysics, Georgian Academy of Sciences, Tbilisi, Georgia*

<sup>3</sup> *INAF – Osservatorio Astronomico di Torino, strada dell’Osservatorio 20, I-10025 Pino Torinese, Italy*

16 November 2018

## ABSTRACT

We investigate mode coupling in a two dimensional compressible disc with radial stratification and differential rotation. We employ the global radial scaling of linear perturbations and study the linear modes in the local shearing sheet approximation. We employ a three-mode formalism and study the vorticity (W), entropy (S) and compressional (P) modes and their coupling properties. The system exhibits asymmetric three-mode coupling: these include mutual coupling of S and P-modes, S and W-modes, and asymmetric coupling between the W and P-modes. P-mode perturbations are able to generate potential vorticity through indirect three-mode coupling. This process indicates that compressional perturbations can lead to the development of vortical structures and influence the dynamics of radially stratified hydrodynamic accretion and protoplanetary discs.

**Key words:** accretion, accretion discs – hydrodynamics – instabilities

## 1 INTRODUCTION

The recent increased interest in the analysis of hydrodynamic disc flows is motivated, on one hand, by the study of turbulent processes, and, on the other, by the investigation of regular structure formation in protoplanetary discs. Indeed, many astrophysical discs are thought to be neutral or having ionization rates too low to effectively couple with magnetic field. Among these are cool and dense areas of protoplanetary discs, discs around young stars, X-ray transient and dwarf nova systems in quiescence (see e.g. Gammie and Menou 1998, Sano et al. 2000, Fromang, Terquem and Balbus 2002). Observational data shows that astrophysical discs often exhibit radial gradients of thermodynamic variables (see e.g. Sandin et al. 2008, Issela et al. 2007). To what extent these inhomogeneities affect the processes occurring in the disc is still subject open to investigations. It has been found that strong local entropy gradients in the radial direction may drive the Rossby wave instability (Lovelace et al. 1999, Li et al. 2000) that transfers thermal to kinetic energy and leads to vortex formation. However, in astrophysical discs, radial stratification is more likely weak. In this case, the radial entropy (temperature) variation on the global scale leads to the existence of baroclinic perturbations over the barotropic equilibrium state. This more appropriate situation has recently become a subject of extensive study.

Klahr and Bodenheimer (2003) pointed out that the radial stratification in the disc can lead to the global baroclinic instability. Numerical results show that the resulting state is highly chaotic and transports angular momentum outwards. Later Klahr (2004) performed a local 2D linear stability analysis of a radially stratified flow with constant surface density and showed that baroclinic perturbations can grow transiently during a limited time interval. John-

son and Gammie (2005) derived analytic solutions for 3D linear perturbations in a radially stratified discs in the Boussinesq approximation. They find that leading and trailing waves are characterized by positive and negative angular momentum flux, respectively. Later Johnson and Gammie (2006) performed numerical simulations, in the local shearing sheet model, to test the radial convective stability and the effects of baroclinic perturbations. They found no substantial instability due to the radial stratification. This result reveals a controversy over the issue of baroclinic instability. Presently, it seems that nonlinear baroclinic instability is an unlikely development in the local dynamics of sub-Keplerian discs with weak radial stratification.

Potential vorticity production, and the formation and development of vortices in radially stratified discs have been studied by Petersen et al. (2007a,b) by using pseudospectral simulations in the anelastic approximation. They show that the existence of thermal perturbations in the radially stratified disc flows leads to the formation of vortices. Moreover, stronger vortices appear in discs with higher temperature perturbations or in simulations with higher Reynolds numbers, and the transport of angular momentum may be both outward and inward.

Keplerian differential rotation in the disc is characterized by a strong velocity shear in the radial direction. It is known that shear flows are non-normal and exhibit a number of transient phenomena due to the non-orthogonal nature of the operators (see e.g. Trefethen et al. 1993). In fact, the studies described above did not take into account the possibility of mode coupling and energy transfer between different modes due to the shear flow induced mode conversion. Mode coupling is inherent to shear flows (cf. Chagelishvili et al. 1995) and often, in many respects, defines the role of perturbation modes in the system dynamics and the further development

arXiv:0909.2844v1 [astro-ph.EP] 15 Sep 2009

of nonlinear processes. Thus, a correct understanding of the energy exchange channels between different modes in the linear regime is vital for a correct understanding of the nonlinear phenomena.

Indications of the shear induced mode conversion can be found in a number of previous studies. Barranco and Marcus 2005 report that vortices are able to excite inertial gravity waves during 3D spectral simulations. Brandenburg and Dintrans (2006) have studied the linear dynamics of perturbation SFH to analyze non-axisymmetric stability in the shearing sheet approximation. Temporal evolution of the perturbation gain factors reveal a wave nature after the radial wavenumber changes sign. Compressible waves are present, along with vortical perturbations, in the simulation by Johnson & Gammie (2005b) but their origin is not particularly discussed.

In parallel, there are a number of papers that focus on the investigation of the shear induced mode coupling phenomena. The study of the linear coupling of modes in Keplerian flows has been conducted in the local shearing sheet approximation (Tevzadze et al. 2003, 2008) as well as in 2D global numerical simulations (Bodo et al. 2005, hereafter B05). Tevzadze et al. (2003) studied the linear dynamics of three-dimensional small scale perturbations (with characteristic scales much less than the disc thickness) in vertically (stably) stratified Keplerian discs. They show, that vortex and internal gravity wave modes are coupled efficiently. B05 performed global numerical simulations of the linear dynamics of initially imposed two-dimensional pure vortex mode perturbations in compressible Keplerian discs with constant background pressure and density. The two modes possible in this system are effectively coupled: vortex mode perturbations are able to generate density-spiral waves. The coupling is, however, strongly asymmetric: the coupling is effective for wave generation by vortices, but not vice-versa. The resulting dynamical picture points out the importance of mode coupling and the necessity of considering compressibility effects for processes with characteristic scales of the order or larger than the disc thickness. Bodo et al. (2007) extended this work to nonlinear amplitudes and found that mode coupling is an efficient channel for energy exchange and is not an artifact of the linear analysis. B05 is particularly relevant to the present study, since it studies the dynamics of mode coupling in 2D unstratified flows and is a good starting point for a further extension to radially stratified flows. Later, Heinemann & Papaloizou (2009a) derived WKB solutions of the generated waves and performed numerical simulations of the wave excitation by turbulent fluctuations (Heinemann & Papaloizou 2009b).

In the present paper we study the linear dynamics of perturbations and analyze shear flow induced mode coupling in the local shearing sheet approximation. We investigate the properties of mode coupling using qualitative analysis within the three-mode approximation. Within this approximation we tentatively distinguish vorticity, entropy and pressure modes. Quantitative results on mode conversion are derived numerically. It seems that a weak radial stratifications, while being a weak factor for the disc stability, still provides an additional degree of freedom (an active entropy mode), opening new options for velocity shear induced mode conversion, that may be important for the system behavior. One of the direct result of mode conversion is the possibility of linear generation of the vortex mode (i.e., potential vorticity) by compressible perturbations. We want to stress the possibility of the coupling between high and low frequency perturbations, considering that high frequency oscillations have been often neglected during previous investigations in particular for protoplanetary discs.

Conventionally there are two distinct viewpoints commonly

employed during the investigation of hydrodynamic astrophysical discs. In one case (self gravitating galactic discs) the emphasis is placed on the investigation of the dynamics of spiral-density waves and vortices, although normally present in numerical simulations, are thought to play a minor role in the overall dynamics. In the other case (non-self-gravitating hydrodynamic discs) the focus is on the potential vorticity perturbations and density-spiral waves are often thought to play a minor role. Here, discussing the possible (multi) mode couplings, we want to draw attention to the possible flaws of these simplified views (see e.g. Mamatsashvili & Chagelishvili 2007). In many cases, mode coupling makes different perturbation to equally participate in the dynamical processes despite of a significant difference in their temporal scales.

In the next section we present mathematical formalism of our study. We describe three mode formalism and give schematic picture of the linear mode coupling in the radially sheared and stratified flow. Numerical analysis of the mode coupling is presented in Sec. 3. We evaluate mode coupling efficiencies at different radial stratification scales of the equilibrium pressure and entropy. The paper is summarized in Sec. 4.

## 2 BASIC EQUATIONS

The governing ideal hydrodynamic equations of a two-dimensional, compressible disc flows in polar coordinates are:

$$\frac{\partial \Sigma}{\partial t} + \frac{1}{r} \frac{\partial (r \Sigma V_r)}{\partial r} + \frac{1}{r} \frac{\partial (\Sigma V_\phi)}{\partial \phi} = 0, \quad (1)$$

$$\frac{\partial V_r}{\partial t} + V_r \frac{\partial V_r}{\partial r} + \frac{V_\phi}{r} \frac{\partial V_r}{\partial \phi} - \frac{V_\phi^2}{r} = -\frac{1}{\Sigma} \frac{\partial P}{\partial r} - \frac{\partial \psi_g}{\partial r}, \quad (2)$$

$$\frac{\partial V_\phi}{\partial t} + V_r \frac{\partial V_\phi}{\partial r} + \frac{V_\phi}{r} \frac{\partial V_\phi}{\partial \phi} + \frac{V_r V_\phi}{r} = -\frac{1}{\Sigma r} \frac{\partial P}{\partial \phi}, \quad (3)$$

$$\frac{\partial P}{\partial t} + V_r \frac{\partial P}{\partial r} + \frac{V_\phi}{r} \frac{\partial P}{\partial \phi} = -\gamma P \left( \frac{1}{r} \frac{\partial (r V_r)}{\partial r} + \frac{1}{r} \frac{\partial V_\phi}{\partial \phi} \right), \quad (4)$$

where  $V_r$  and  $V_\phi$  are the flow radial and azimuthal velocities respectively.  $P(r, \phi)$ ,  $\Sigma(r, \phi)$  and  $\gamma$  are respectively the pressure, the surface density and the adiabatic index.  $\psi_g$  is the gravitational potential of the central mass, in the absence of self-gravitation ( $\psi_g \sim -1/r$ ). This potential determines the Keplerian angular velocity:

$$\frac{\partial \psi_g}{\partial r} = \Omega_{Kep}^2 r, \quad \Omega_{Kep} \sim r^{-3/2}; \quad (5)$$

### 2.1 Equilibrium state

We consider an axisymmetric ( $\partial/\partial\phi \equiv 0$ ), azimuthal ( $\bar{V}_r = 0$ ) and differentially rotating basic flow:  $\bar{V}_\phi = \Omega(r)r$ . In the 2D radially stratified equilibrium (see Klahr 2004), all variables are assumed to follow a simple power law behavior:

$$\bar{\Sigma}(r) = \Sigma_0 \left( \frac{r}{r_0} \right)^{-\beta_\Sigma}, \quad \bar{P}(r) = P_0 \left( \frac{r}{r_0} \right)^{-\beta_P}, \quad (6)$$

where overbars denote equilibrium and  $\Sigma_0$  and  $P_0$  are the values of the equilibrium surface density and pressure at some fiducial radius  $r = r_0$ . The entropy can be calculated as:

$$\bar{S} = \bar{P} \bar{\Sigma}^{-\gamma} = - \left( \frac{r}{r_0} \right)^{-\beta_S}, \quad (7)$$

where

$$\beta_S \equiv \beta_P - \gamma\beta_\Sigma. \quad (8)$$

$S$  is sometimes called potential temperature, while the physical entropy can be derived as  $\bar{S} = C_V \log S + \bar{S}_0$ .

This equilibrium shows a deviation from the Keplerian profile due to the radial stratification:

$$\begin{aligned} \Delta\Omega^2(r) &= \Omega^2(r) - \Omega_{Kep}^2 = \frac{1}{r\bar{\Sigma}(r)} \frac{\partial \bar{P}(r)}{\partial r} = \\ &= -\frac{P_0}{\Sigma_0} \frac{\beta_P}{r_0^2} \left(\frac{r}{r_0}\right)^{\beta_\Sigma - \beta_P - 2}. \end{aligned} \quad (9)$$

Hence, the described state is sub-Keplerian or super-Keplerian when the radial gradient of pressure is negative ( $\beta_P > 0$ ) or positive ( $\beta_P < 0$ ), respectively. Although these discs are non-Keplerian, they are still rotationally supported, since the deviation from the Keplerian profile is small:  $\Delta\Omega^2(r) \ll \Omega_{Kep}^2$ .

## 2.2 Linear perturbations

We split the physical variables into mean and perturbed parts:

$$\Sigma(r, \phi) = \bar{\Sigma}(r) + \Sigma'(r, \phi), \quad (10)$$

$$P(r, \phi) = \bar{P}(r) + P'(r, \phi), \quad (11)$$

$$V_r(r, \phi) = V_r'(r, \phi), \quad (12)$$

$$V_\phi(r, \phi) = \Omega(r)r + V_\phi'(r, \phi). \quad (13)$$

In order to remove background trends from the perturbations we employ the global radial power law scaling for perturbed quantities:

$$\hat{\Sigma}(r) \equiv \left(\frac{r}{r_0}\right)^{-\delta_\Sigma} \Sigma'(r), \quad (14)$$

$$\hat{P}(r) \equiv \left(\frac{r}{r_0}\right)^{-\delta_P} P'(r), \quad (15)$$

$$\hat{\mathbf{V}}(r) \equiv \left(\frac{r}{r_0}\right)^{-\delta_V} \mathbf{V}'(r). \quad (16)$$

After the definitions one can get the following dynamical equations for the scaled perturbed variables:

$$\left\{ \frac{\partial}{\partial t} + \Omega(r) \frac{\partial}{\partial \phi} \right\} \frac{\hat{\Sigma}}{\Sigma_0} + \quad (17)$$

$$\begin{aligned} \left(\frac{r}{r_0}\right)^{-\beta_\Sigma - \delta_\Sigma + \delta_V} \left[ \frac{\partial \hat{V}_r}{\partial r} + \frac{1}{r} \frac{\partial \hat{V}_\phi}{\partial \phi} + \frac{1 + \delta_V - \beta_\Sigma}{r} \hat{V}_r \right] = 0, \\ \left\{ \frac{\partial}{\partial t} + \Omega(r) \frac{\partial}{\partial \phi} \right\} \hat{V}_r - 2\Omega(r) \hat{V}_\phi + \end{aligned} \quad (18)$$

$$\begin{aligned} \frac{c_s^2}{\gamma} \left(\frac{r}{r_0}\right)^{\beta_\Sigma + \delta_P - \delta_V} \frac{\partial \hat{P}}{\partial r} \frac{1}{P_0} + c_s^2 \frac{\delta_P}{\gamma r_0} \left(\frac{r}{r_0}\right)^{\beta_\Sigma + \delta_P - \delta_V - 1} \frac{\hat{P}}{P_0} + \\ c_s^2 \frac{\beta_P}{\gamma r_0} \left(\frac{r}{r_0}\right)^{2\beta_\Sigma + \delta_\Sigma - \beta_P - \delta_V - 1} \frac{\hat{\Sigma}}{\Sigma_0} = 0, \\ \left\{ \frac{\partial}{\partial t} + \Omega(r) \frac{\partial}{\partial \phi} \right\} \hat{V}_\phi + \left( 2\Omega(r) + r \frac{\partial \Omega(r)}{\partial r} \right) \hat{V}_r + \end{aligned} \quad (19)$$

$$\frac{c_s^2}{\gamma r_0} \left(\frac{r}{r_0}\right)^{\beta_\Sigma + \delta_P - \delta_V - 1} \frac{\partial \hat{P}}{\partial \phi} \frac{1}{P_0} = 0, \quad (20)$$

$$\left\{ \frac{\partial}{\partial t} + \Omega(r) \frac{\partial}{\partial \phi} \right\} \frac{\hat{P}}{P_0} + \quad (20)$$

$$\gamma \left(\frac{r}{r_0}\right)^{-\beta_P + \delta_V - \delta_P} \left[ \frac{\partial \hat{V}_r}{\partial r} + \frac{1}{r} \frac{\partial \hat{V}_\phi}{\partial \phi} + \frac{1 + \delta_V - \beta_P / \gamma}{r} \hat{V}_r \right] = 0,$$

where  $c_s^2 = \gamma P_0 / \Sigma_0$  is the squared sound speed at  $r = r_0$ .

## 2.3 Local approximation

The linear dynamics of perturbations in differentially rotating flows can be effectively analyzed in the local co-rotating shearing sheet frame (e. g., Goldreich & Lynden-Bell 1965; Goldreich & Tremaine 1978). This approximation simplifies the mathematical description of flows with inhomogeneous velocity. In the radially stratified flows the spatial inhomogeneity of the governing equations comes not only from the equilibrium velocity, but from the pressure, density and entropy profiles as well. In this case we first re-scale perturbations in global frame in order to remove background trends from linear perturbations, rather than use complete form of perturbations to the equilibrium (see Eqs. 14-16). Hence, using the re-scaled linear perturbation ( $\hat{P}$ ,  $\hat{\Sigma}$ ,  $\hat{\mathbf{V}}$ ) we may simplify local shearing sheet description as follows. Introduction of a local Cartesian co-ordinate system:

$$x \equiv r - r_0, \quad y \equiv r_0(\phi - \Omega_0 t), \quad \frac{x}{r_0}, \frac{y}{r_0} \ll 1, \quad (21)$$

$$\frac{\partial}{\partial x} = \frac{\partial}{\partial r}, \quad \frac{\partial}{\partial y} = \frac{1}{r_0} \frac{\partial}{\partial \phi}, \quad \frac{\partial}{\partial t} = \frac{\partial}{\partial t} - r_0 \Omega_0 \frac{\partial}{\partial y}, \quad (22)$$

where  $\Omega_0$  is the local rotation angular velocity at  $r = r_0$ , transforms global differential rotation into a local radial shear flow and the two Oort constants define the local shear rate:

$$A \equiv \frac{1}{2} r_0 \left[ \frac{\partial \Omega(r)}{\partial r} \right]_{r=r_0}, \quad (23)$$

$$B \equiv -\frac{1}{2} \left[ r \frac{\partial \Omega(r)}{\partial r} + 2\Omega(r) \right]_{r=r_0} = -A - \Omega_0. \quad (24)$$

Hence, the equations describing the linear dynamics of perturbations in local approximation read as follows:

$$\left\{ \frac{\partial}{\partial t} + 2Ax \frac{\partial}{\partial y} \right\} \frac{\hat{P}}{\gamma P_0} + \quad (25)$$

$$\begin{aligned} \left[ \frac{\partial \hat{V}_x}{\partial x} + \frac{\partial \hat{V}_y}{\partial y} + \frac{1 + \delta_V - \beta_P / \gamma}{r_0} \hat{V}_x \right] = 0, \\ \left\{ \frac{\partial}{\partial t} + 2Ax \frac{\partial}{\partial y} \right\} \hat{V}_x - 2\Omega_0 \hat{V}_y + \end{aligned} \quad (26)$$

$$c_s^2 \left[ \frac{\partial \hat{P}}{\partial x} \frac{1}{\gamma P_0} + \frac{\delta_P + \beta_P / \gamma}{r_0} \frac{\hat{P}}{\gamma P_0} - \frac{\beta_P}{\gamma r_0} \frac{\hat{S}}{\gamma P_0} \right] = 0,$$

$$\left\{ \frac{\partial}{\partial t} + 2Ax \frac{\partial}{\partial y} \right\} \hat{V}_y - 2B \hat{V}_y + c_s^2 \frac{\partial \hat{P}}{\partial y} \frac{1}{\gamma P_0} = 0, \quad (27)$$

$$\left\{ \frac{\partial}{\partial t} + 2Ax \frac{\partial}{\partial y} \right\} \frac{\hat{S}}{\gamma P_0} - \frac{\beta_S}{\gamma r_0} \hat{V}_x = 0, \quad (28)$$

where  $\hat{S}$  is the entropy perturbation:

$$\hat{S} \equiv \hat{P} - c_s^2 \hat{\Sigma}. \quad (29)$$

Now we may adjust the global scaling law of perturbations in order to simplify the local shearing sheet description (see Eqs. 25,26):

$$1 + \delta_V - \beta_P / \gamma = 0, \quad (30)$$

$$\delta_P + \beta_P/\gamma = 0. \quad (31)$$

Let us introduce spatial Fourier harmonics (SFHs) of perturbations with time dependent phases:

$$\begin{pmatrix} \hat{V}_x(\mathbf{r}, t) \\ \hat{V}_y(\mathbf{r}, t) \\ \hat{P}(\mathbf{r}, t)/\gamma P_0 \\ \hat{S}(\mathbf{r}, t)/\gamma P_0 \end{pmatrix} = \begin{pmatrix} u_x(\mathbf{k}(t), t) \\ u_y(\mathbf{k}(t), t) \\ -ip(\mathbf{k}(t), t) \\ s(\mathbf{k}(t), t) \end{pmatrix} \times \exp(ik_x(t)x + ik_y y), \quad (32)$$

with

$$k_x(t) = k_x(0) - 2Ak_y t. \quad (33)$$

Using the above expansion and Eqs. (27-30), we obtain a compact ODE system that governs the local dynamics of SFHs of perturbations:

$$\frac{d}{dt}p - k_x(t)u_x - k_y u_y = 0, \quad (34)$$

$$\frac{d}{dt}u_x - 2\Omega_0 u_y + c_s^2 k_x(t)p - c_s^2 k_P s = 0, \quad (35)$$

$$\frac{d}{dt}u_y - 2Bu_x + c_s^2 k_y p = 0, \quad (36)$$

$$\frac{d}{dt}s - k_s u_x = 0. \quad (37)$$

where

$$k_P = \frac{\beta_P}{\gamma r_0} \quad k_S = \frac{\beta_S}{\gamma r_0}. \quad (38)$$

The potential vorticity:

$$W \equiv k_x(t)u_y - k_y u_x - 2Bp, \quad (39)$$

is a conserved quantity in barotropic flows:  $W = \text{const.}$  when  $k_P = 0$ .

## 2.4 Perturbations at rigid rotation

The dispersion equation of our system can be obtained in the shearless limit ( $A = 0$ ,  $B = -\Omega$ ). Hence, using Fourier expansion of perturbations in time  $\propto \exp(i\omega t)$ , in the shearless limit, we obtain:

$$\omega^4 - (c_s^2 k^2 + 4\Omega_0^2 - c_s^2 \eta) \omega^2 - c_s^4 \eta k_y^2 = 0, \quad (40)$$

where

$$\eta \equiv k_P k_S = \frac{\beta_P \beta_S}{\gamma^2 r_0^2}. \quad (41)$$

Solutions of the Eq. (40) describe a compressible density-spiral mode and a convective mode that involves perturbations of entropy and potential vorticity. For weakly stratified discs ( $\eta \ll k^2$ ), we find the frequencies are:

$$\bar{\omega}_p^2 = c_s^2 k^2 + 4\Omega_0^2, \quad (42)$$

$$\bar{\omega}_c^2 = -\frac{c_s^4 \eta k_y^2}{c_s^2 k^2 + 4\Omega_0^2}. \quad (43)$$

High frequency solutions ( $\bar{\omega}_p^2$ ) describe the density-spiral waves and will be referred later as the P-modes. Low frequency solutions ( $\bar{\omega}_c^2$ ), instead, describe radial buoyancy mode due to the stratification. In barotropic flows ( $\eta = 0$ ) this mode is degenerated into stationary zero frequency vortical solution. Therefore, we may refer to it as a baroclinic mode. The mode describes instability when  $\eta > 0$ .

In this case the equilibrium pressure and entropy gradients point in the same direction. Klahr (2004) has anticipated such result, although worked in the constant surface density limit ( $\beta_S = 0$ ). The same behavior has been obtained for axisymmetric perturbations in Johnson and Gammie (2005). For comparison, in our model baroclinic perturbations are intrinsically non-axisymmetric. Hence, our result obtained in the rigidly rotating limit shows that the local exponential stability of the radial baroclinic mode is defined by the Schwarzschild-Ledoux criterion:

$$\frac{d\bar{P}}{dr} \frac{d\bar{S}}{dr} > 0. \quad (44)$$

The dynamics of linear modes can be described using the modal equations for the eigenfunctions:

$$\left\{ \frac{d^2}{dt^2} + \bar{\omega}_{p,c}^2 \right\} \Phi_{p,c}(t) = 0, \quad (45)$$

where  $\Phi_p(t)$  and  $\Phi_c(t)$  are the eigenfunctions of the pressure and convective (baroclinic) modes, respectively. The form of these functions can be derived from Eqs. (34-41) in the shearless limit:

$$\Phi_{p,c}(t) = (\bar{\omega}_{p,c}^2 + c_s^2 \eta) p(t) - 2\Omega_0 W(t) - c_s^2 k_P k_x s(t). \quad (46)$$

All physical variables in our system ( $p$ ,  $u_x$ ,  $u_y$ ,  $s$ ) can be expressed by the two modal eigenfunctions and their first time derivatives ( $\Phi_{p,c}$ ,  $\Phi'_{p,c}$ ). Hence, we can fully derive the perturbation field of a specific mode individually by setting the eigenfunction of the other mode equal to zero.

As we will see later, the Keplerian shear leads to the degeneracy of the convective buoyancy mode. In this case only the shear modified density-spiral wave mode eigenfunction can be employed in the analysis.

## 2.5 Perturbations in shear flow: mode coupling

It is well known that velocity shear introduces non-normality into the governing equations that significantly affects the dynamics of different perturbations. In this case we benefit from the shearing sheet transformation and seek the solutions in the form of the so-called Kelvin modes. These originate from the vortical solutions derived in seminal paper by Kelvin (1887). In fact, as it was argued lately (see e.g., Volponi and Yoshida 2002), the shearing sheet transformation leads to some sort of generalized modal approach. Shear modes arising in such description differ from linear modes with exponential time dependence in many respects. Primarily, phases of these continuous spectrum shear modes vary in time through shearing wavenumber; their amplitudes can be time dependent; and most importantly, they can couple in limited time intervals. On the other hand, shear modes can be well separated asymptotically, where analytic WKBJ solution for the each mode can be increasingly accurate. In the following, we will simply refer to these shearing sheet solution as ‘‘modes’’.

The character of shear flow effects significantly depend on the value of velocity shear parameter. To estimate the time-scales of the processes we compare the characteristic frequencies of the linear modes  $|\bar{\omega}_p|$ ,  $|\bar{\omega}_c|$  and the velocity shear  $|A|$ . In order to speak about the modification of the linear mode by the velocity shear, the basic frequency of the mode should be higher than the one set by shear itself:  $\omega^2 > A^2$ . Otherwise the modal solution can not be used to calculate perturbation dynamics, since perturbations will obey the shear induced variations at shorter timescales.

In quasi-Keplerian differentially rotating discs with weak radial stratification:

$$\bar{\omega}_p^2 \gg A^2 \quad \text{and} \quad \bar{\omega}_c^2 \ll A^2, \quad \text{when} \quad \frac{\beta_P \beta_S}{\gamma^2} \ll 1. \quad (47)$$

In this case the convective mode diverges from its modal behavior and is strongly affected by the velocity shear: the thermal and kinematic parts obey shear driven dynamics individually. Therefore, we tentatively distinguish shear driven vorticity (W) and entropy (S) modes. On the contrary, the high frequency pressure mode is only modified by the action of the background shear. Hence, we assume the above described three mode (S, W and P) formalism as the framework for our further study.

For the description of the P mode in differential rotation we define the function:

$$\Psi_p(t) = \omega_p^2(t)p(t) - 2\Omega_0 W(t) - c_s^2 k_P k_x(t)s(t), \quad (48)$$

where

$$\omega_p^2(t) = c_s^2 k^2(t) - 4B\Omega_0. \quad (49)$$

This can be considered as the generalization of the  $\Phi_P(t)$  eigenfunction for the case of the shear flow, by accounting for the temporal variation of the radial wavenumber.

In order to analyze the mode coupling in the considered limit, we rewrite Eqs. (34-39) as follows:

$$\left\{ \frac{d^2}{dt^2} + f_p \frac{d}{dt} + \omega_p^2 - \Delta\omega_p^2 \right\} \Psi_p = \chi_{pw} W + \chi_{ps} S, \quad (50)$$

$$\left\{ \frac{d}{dt} + f_s \right\} S = \chi_{sp1} \frac{d\Psi_p}{dt} + \chi_{sp2} \Psi_p + \chi_{sw} W, \quad (51)$$

$$\frac{dW}{dt} = \chi_{ws} S, \quad (52)$$

where  $f_p$  and  $\Delta\omega_p^2$  describe the shear flow induced modification to the P-mode

$$f_p = 4A \frac{k_x k_y}{k^2} - 2 \frac{(\omega_p^2)'}{\omega_p^2}, \quad (53)$$

$$\Delta\omega_p^2 = \frac{(\omega_p^2)''}{\omega_p^2} + f_p \frac{(\omega_p^2)'}{\omega_p^2} + 8AB \frac{k_y^2}{k^2}, \quad (54)$$

parameter  $f_s$  describes the modification to the entropy mode

$$f_s = c_s^2 \eta \frac{k_x^2 (\omega_p^2)'}{k^2 \omega_p^4}, \quad (55)$$

and  $\chi$  parameters describe the coupling between the different modes:

$$\chi_{pw} = 2\Omega_0 \Delta\omega_p^2(t) + 4A \frac{k_y^2}{k^2} \omega_p^2, \quad (56)$$

$$\chi_{ps} = c_s^2 k_P k_x \left( \Delta\omega_p^2 + 4B \frac{k_y}{k_x} \frac{(\omega_p^2)'}{\omega_p^2} - 8AB \frac{k_y^2}{k^2} \right), \quad (57)$$

$$\chi_{sp1} = \frac{k_S k_x}{k^2 \omega_p^2}, \quad (58)$$

$$\chi_{sp2} = -\frac{k_S k_x}{k^2 \omega_p^2} \left( \frac{(\omega_p^2)'}{\omega_p^2} + 2B \frac{k_y}{k_x} \right), \quad (59)$$

$$\chi_{sw} = -\frac{2\Omega k_S k_x}{k^2 \omega_p^2} \left( \frac{(\omega_p^2)'}{\omega_p^2} + 2B \frac{k_y}{k_x} + \frac{k_y \omega_p^2}{2\Omega k_x} \right), \quad (60)$$

$$\chi_{ws} = -c_s^2 k_P k_y. \quad (61)$$

Here prime denotes temporal derivative.

Equations (50-52) describe the linear dynamics of modes and their coupling in the considered three mode model. In this limit,

our interpretation is that the homogeneous parts of the equations describe the individual dynamics of modes, while the right hand side terms act as a source terms and describe the mode coupling. This tentative separation is already fruitful in a qualitative description of mode coupling.

Dynamics of the density-spiral wave mode in the differential rotation can be described by the homogeneous part of the Eq. (50). Homogeneous part of Eq. (51) describes the modifications to the entropy dynamics. Inhomogeneous parts of the Eqs. (50-52) reveal coupling terms between the three linear modes that originate due to the background velocity shear and radial stratification. We analyze the mode coupling dynamics numerically, but use the coupling  $\chi$  coefficients for qualitative description.

The sketch illustration of the mode coupling in the above described three-mode approximation can be seen in Fig. 1. The figure reveals a complex picture of the three mode coupling that originates by the combined action of velocity shear and radial stratification.

The temporal variation of the coupling coefficients during the swing of the perturbation SFHs from leading to trailing phases is shown in Fig. 2. The relative amplitudes of the  $\chi_{pw}$  and  $\chi_{ps}$  parameters reveal that potential vorticity is a somewhat more effective source of P mode perturbations when compared to the entropy mode. On the other hand, it seems that S mode excitation sources due to potential vorticity ( $\chi_{sw}$ ) can be stronger when compared with the P-mode sources ( $\chi_{sp1}$ ,  $\chi_{sp2}$ ).

The effect of the stratification parameters on the mode coupling is somewhat more apparent. First, we may conclude that the excitation of the entropy mode, which depends on the parameters  $\chi_{sp1}$ ,  $\chi_{sp2}$  and  $\chi_{sw}$  is generally a stronger process for higher entropy stratification scales  $k_S$  (see Eqs. 58-60). Second, we see that the generation of the potential vorticity depending on the  $\chi_{ws}$  parameter proceeds more effectively at high pressure stratification scale  $k_P$ . And third, we see profound asymmetry in the three-mode coupling: P-mode is not coupled with the W-mode *directly*.

A quantitative estimate of the mode excitation parameters can be done using a numerical analysis. In this case, the amplitudes of the generated W and S modes can be estimated through the values of potential vorticity or entropy outside the coupling area. In order to quantify the second order P mode dynamics we define its modal energy as follows:

$$E_P(t) \equiv |\Psi_p(t)|^2 + \omega_p(t)^2 |\Psi_P(t)|^2. \quad (62)$$

This quadratic form is a good approximation to the P mode energy in the areas where it obeys adiabatic dynamics:  $k_x(t)/k_y \gg 1$ .

The presented qualitative analysis suggests that perturbations of the density-spiral waves can generate entropy perturbations not only due to the flow viscosity (not included in our formalism), but also kinematically, due to the velocity shear induced mode coupling. The generated entropy perturbations should further excite potential vorticity through baroclinic coupling. Hence, it seems that in baroclinic flows, contrary to the barotropic case, P-mode perturbations are able to generate potential vorticity through a three-mode coupling mechanism:  $P \rightarrow S \rightarrow W$ . We believe that traces of the described mode coupling can be also seen in Klahr 2004, where the process has not been fully resolved due to the numerical filters used to remove higher frequency oscillations.

### 3 NUMERICAL RESULTS

In order to study the mode coupling dynamics in more detail we employ numerical solutions of Eqs. (34-37). We impose initial con-

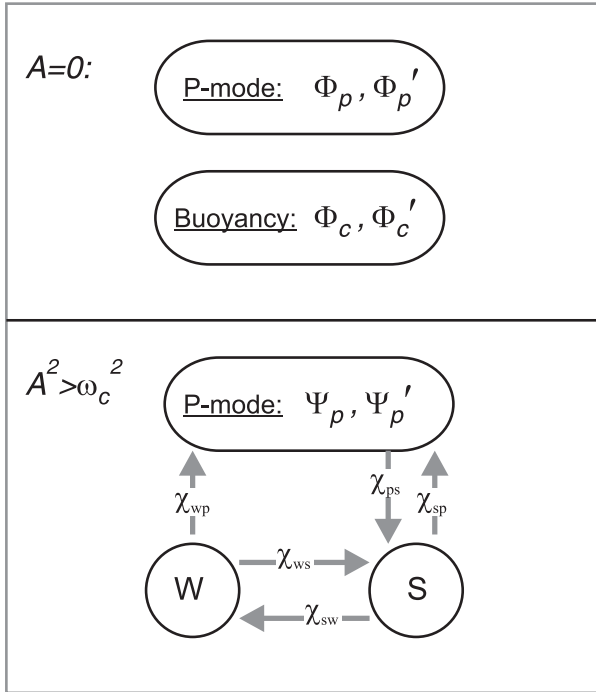


**Figure 1.** Mode coupling scheme. In the zero shear limit two second order modes P-mode and buoyancy mode with eigenfunctions  $\Phi_p$  and  $\Phi_c$  are uncoupled. In the shear flow, when the characteristic time of shearing is shorter than the buoyancy mode temporal variation scale ( $A^2 > \omega_c^2$ ), we use three mode formalism. In this limit we consider the coupling of the P, W, and S modes.  $\chi$  parameters describe the strength of the coupling channel. Asymmetry of the mode coupling is revealed in the fact that compressible oscillations of the pressure mode are not able to directly generate potential vorticity, but still do so via interaction with S-mode and farther baroclinic ties with W-mode.

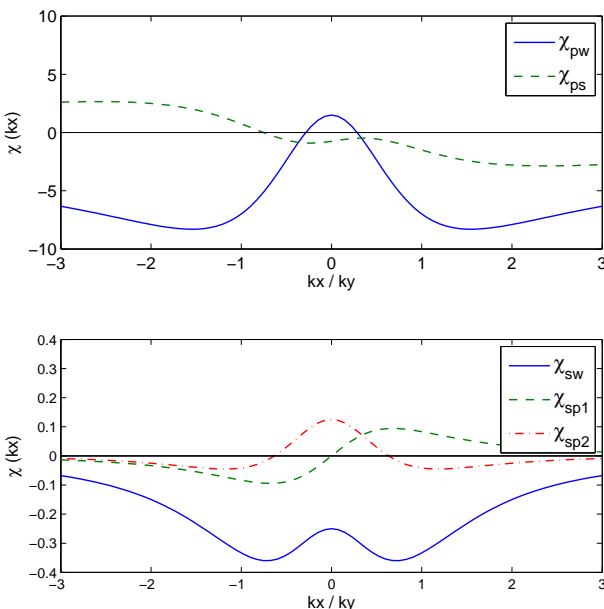


**Figure 2.** The coupling  $\chi$  parameters vs. the ratio of radial to azimuthal wavenumbers  $k_x(t)/k_y$  when latter passes through zero value during the time interval  $\Delta t = 4\Omega_0^{-1}$ . Here  $k_y = H^{-1}$ ,  $k_P = k_S = 0.5H^{-1}$ .

ditions that correspond to the one of the three modes and use a standard Runge-Kutta scheme for numerical integration (MATLAB ode34 RK implementation). Perturbations corresponding to the individual modes at the initial point in time are derived in the Appendix A.

### 3.1 W-mode: direct coupling with S and P-modes

In this subsection we consider the dynamics of SFH when only the perturbations of potential vorticity are imposed initially. As it is known from previous studies (see Chagelishvili et al. 1997, Bodo et al. 2005) vorticity perturbations are able to excite acoustic modes nonadiabatically in the vicinity of the area where  $k_x(t) = 0$ . Here we observe a similar, but more complex, behavior of mode coupling. The W-mode is able to generate P and S-modes simultaneously. Fig. 3 shows the evolution of the W-mode perturbations in a flow with growing baroclinic perturbations ( $\eta > 0$ ). The results show the excitation of both S and P-mode perturbations due to mode coupling that occurs in a short period of time in the vicinity of  $t = 10$ . The following growth of the negative potential vorticity is due to the baroclinic coupling of entropy and potential vorticity perturbations.

Fig. 4 shows the evolution of potential vorticity SFH in flows with negative  $\eta$ . After the mode coupling and generation of P and S-modes, we observe a decrease of potential vorticity. This represents the well known fact that stable stratification (positive Richardson number) can play a role of “baroclinic viscosity” on the vorticity perturbations.

Numerical calculations show that the efficiency of the mode coupling generally decreases as we increase the azimuthal wavenumber  $k_y$  corresponding to an increase of the density-spiral wave frequency: lower frequency waves couple more efficiently.

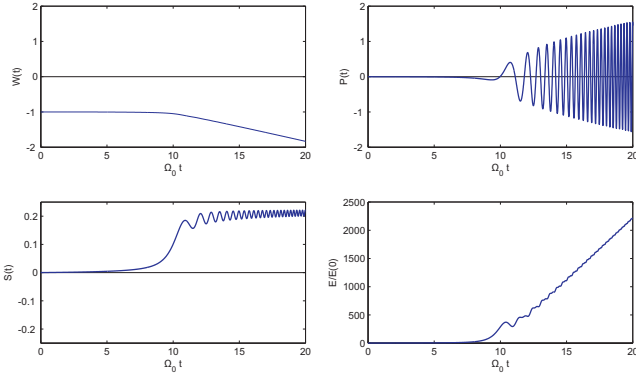
To test the effect of background stratification parameters on the mode coupling, we calculate the amplitude of the entropy and the energy of the P-mode perturbations generated in flows with different pressure and entropy stratification scales. The amplitudes are calculated after a  $10\Omega_0^{-1}$  time interval from the change in sign of the radial wave-number. In this case, modes are well isolated and the energy of the P mode can be well defined.

Fig. 5 shows the results of these calculations. It seems that the mode coupling efficiency is higher with stronger radial gradients. In particular, numerical results generally verify our qualitative results that the S-mode generation predominantly depends on the entropy stratification scale  $k_S$ . Therefore, P-mode excitation is stronger for higher values of  $\eta$ .

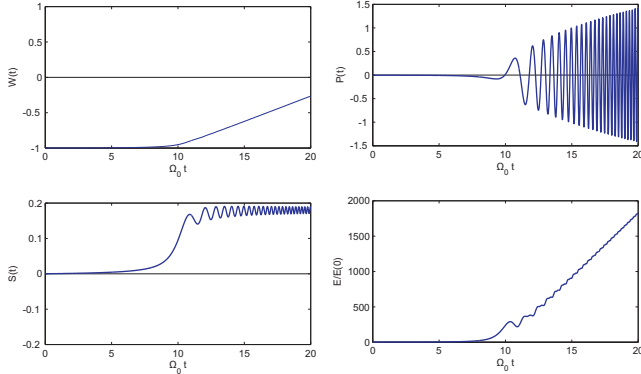
### 3.2 S-mode: direct coupling with W and P-modes

Fig. 6 shows the evolution of the S-mode SFH in a flow with growing baroclinic perturbations. Here we observe two shear flow phenomena: mode coupling and transient amplification. Entering the nonadiabatic area (around  $t = 10$ ) the entropy SFH is able to generate the P-mode, while undergoing transient amplification itself. The transient growth of entropy is unsubstantial and the growth rate decreases with the growth of  $k_y$ . The W-mode is instead constantly coupled to entropy perturbations through baroclinic forces, although higher entropy perturbations at later times give an higher rate of growth of potential vorticity. The total energy of perturbations is however dominated, at the end, by the P mode.

Fig. 7 shows the dependence of the W and P-mode generation on the pressure and entropy stratification scales. As expected from



**Figure 3.** Evolution of the W-mode SFH in the flow with  $k_x(t) = -30H^{-1}$ ,  $k_y = 2H^{-1}$  and equilibrium with growing baroclinic perturbations  $k_P = k_S = 0.2H^{-1}$ . Mode coupling occurs in the vicinity of  $t = 10\Omega_0^{-1}$ , where  $k_x(t) = 0$ . Excitation of the P and S-modes are clearly seen in the panels for pressure ( $P$ ) and entropy ( $S$ ) perturbations. Perturbations of the potential vorticity start to grow due to the baroclinic coupling with entropy perturbations.



**Figure 4.** Evolution of the W-mode SFH in the flow with  $k_x(t) = -30H^{-1}$ ,  $k_y = 2H^{-1}$  and equilibrium with positive  $\eta$ :  $k_P = -0.2H^{-1}$ ,  $k_S = 0.2H^{-1}$ . Interestingly, SFH dynamics shows the decay of potential vorticity after the mode coupling and excitation of S- and W-modes at  $t = 10\Omega_0^{-1}$ . The latter fact is normally anticipated process in the flows that are baroclinically stable.

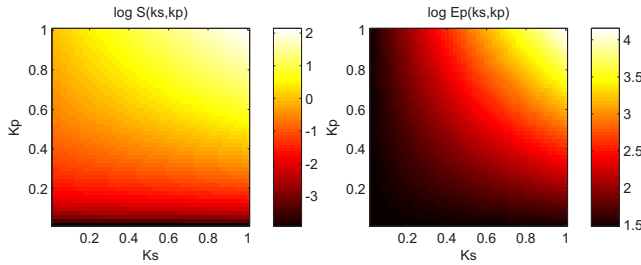


**Figure 5.** Surface graph of the generated S and P-mode amplitudes at  $k_y = 2H^{-1}$ ,  $k_x = -60H^{-1}$ , and different values of  $k_P$  and  $k_S$ . Initial perturbations are normalized to set  $E(0)=1$ . Excitation amplitudes of the entropy perturbations show stronger dependence of the  $k_S$  (left panel), while both entropy and pressure scales are important (approximately  $k_S k_P$  dependence) for the generation of P-modes (right panel). See electronic edition of the journal for color images.

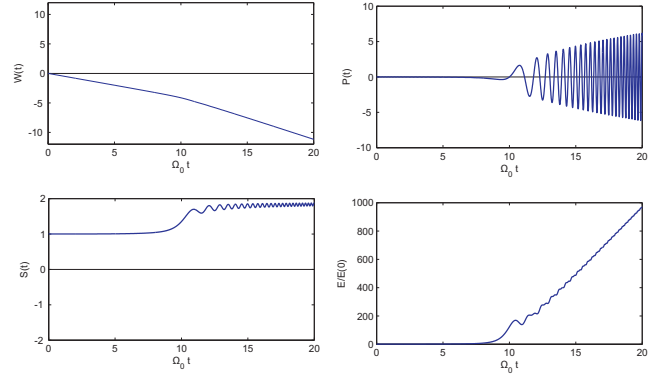


**Figure 6.** Evolution of the S-mode SFH in the flow with  $k_x(t) = -30H^{-1}$ ,  $k_y = 2H^{-1}$  and equilibrium with growing baroclinic perturbations  $k_P = k_S = 0.2H^{-1}$ . Perturbations of the potential vorticity are coupled grow from the beginning due to the baroclinic coupling with entropy perturbations. Excitation of the P-mode is clearly seen in the panel for pressure ( $P$ ), while the panel for entropy perturbations ( $S$ ) shows swing amplification in the nonadiabatic area around  $k_x(t) = 0$ . Change of the amplitude of the entropy SFH affects the growth factor of potential vorticity SFH.

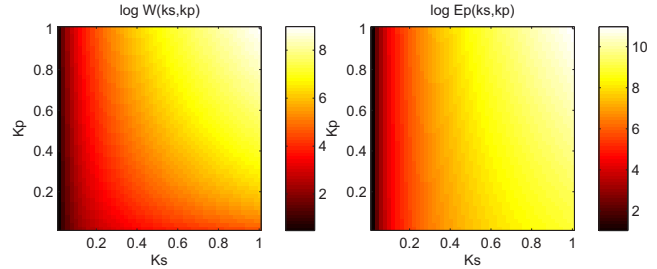


**Figure 7.** Surface graph of the generated W and P-mode amplitudes at  $k_y = 2H^{-1}$ ,  $k_x = -60H^{-1}$ , and different values of  $k_P$  and  $k_S$ . Initial perturbations are normalized to set  $E(0)=1$ . Excitation amplitudes of the entropy perturbations show predominant dependence on the  $k_S$  (left panel), while only pressure stratification scale  $k_P$  is important for the generation of P-modes (right panel). See electronic edition of the journal for color images.

qualitative estimates, P-mode excitation depends almost solely on the pressure stratification scale  $k_P$ , while the generation of potential vorticity generally grows with  $\eta$ .

### 3.3 P-mode: direct coupling with S-mode and indirect coupling with W-mode

Fig. 8 shows the evolution of an initially imposed P-mode SFH in a flow with growing baroclinic perturbations. The *oscillating* behavior of the entropy perturbation for  $t < 10$  is given by the P-mode. This oscillating component has a zero mean value when averaged over time-scales longer than the wave period. The existence of the *aperiodic* S-mode is instead characterized by a nonzero mean value. When the azimuthal wavenumber  $k_y(t)$  changes sign at  $t = 10$ , we can observe the appearance of a nonzero mean value (marked on the plot by the horizontal dashed line), indicating that the high frequency oscillations of the P-mode are able to generate the aperiodic perturbations of the S-mode. The aperiodic part of the entropy perturbation is than able to generate potential vorticity perturbations. However, as we see from Eq. (54) and Fig. 1,

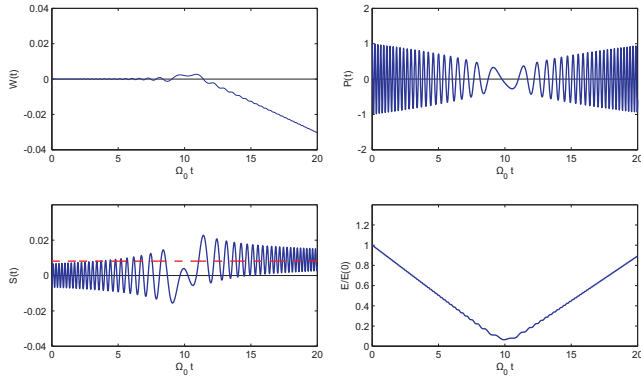


**Figure 8.** Evolution of the P-mode SFH in the flow with  $k_x(t) = -30H^{-1}$ ,  $k_y = 2H^{-1}$  and equilibrium with growing baroclinic perturbations  $k_P = k_S = 0.2H^{-1}$ . Mode coupling occurs in the vicinity of  $t = 10\Omega_0^{-1}$ , where W and S-modes are excited. The amplitude of the generated aperiodic contribution to the entropy perturbation is marked by the red dotted line. Farther, this component leads to the baroclinic production of potential vorticity with negative sign.

there is no direct coupling between P and W-modes. Therefore, the P-mode generates the S-mode by shear flow induced mode conversion, while the W-mode is further generated because of its baroclinic ties with the entropy SFH. We describe this situation as the three-mode coupling or in other words, indirect coupling of the P to the W-mode. Note, that although the S and W-mode generation is apparent from the dynamics of entropy and potential vorticity SFH, energetically it plays a minor role as compared to the compressible energy carried by the P-mode.

Fig 9. shows that P-mode generates potential vorticity with a positive sign. However, the sign of the generated potential vorticity depends on the initial phase of the P-mode. Hence, our numerical results show generation of the W-mode with both positive and negative signs.

It is interesting also to look at the P-mode dynamics in flows stable to baroclinic perturbations (see Fig. 9). The initially imposed P-mode is able to generate the S-mode and consequently the W-mode, that gives a growth of the potential vorticity with time. Apart from the intrinsic limitations (the dependence of the sign of the generated potential vorticity on the initial phase of the P-mode and the low efficiency of the W-mode generation), this process demonstrates the fact that potential vorticity can be actually generated in flows with positive radial buoyancy ( $\eta < 0$ ) and Richardson number.

Fig. 10 shows the dependence of the S and W-mode generation on the pressure and entropy stratification scales. In good agreement with qualitative estimates, the S-mode excitation depends strongly on the entropy stratification scale  $k_S$ , while the generation of the potential vorticity generally grows with  $\eta$ .

#### 4 CONCLUSION AND DISCUSSION

We have studied the dynamics of linear perturbations in a 2D, radially stratified, compressible, differentially rotating flow with different radial density, pressure and entropy gradients. We employed global radial scaling of linear perturbations and removed the algebraic modulation due to the background stratification. We derived a local dispersion equation for nonaxisymmetric perturbations and the corresponding eigenfunctions in the zero shear limit. We show

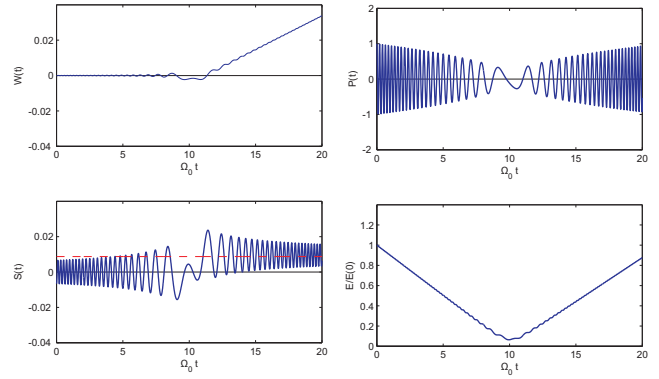


**Figure 9.** Same as in previous figure but for  $k_P = -0.2H^{-1}$  and  $k_S = 0.2H^{-1}$ . Perturbations are stable to baroclinic forces. However, production of the potential vorticity with positive sign is still observed.

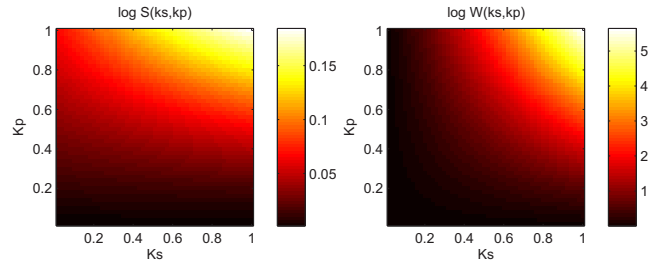


**Figure 10.** Surface graph of the generated S and W-mode amplitudes at  $k_y = 2H^{-1}$ ,  $k_x = -60H^{-1}$ , and different values of  $k_P$  and  $k_S$ . Initial perturbations are normalized to set  $E(0)=1$ . Excitation amplitudes of the entropy perturbations mainly depend on the  $k_S$  (left panel), while both pressure and entropy stratification scales are important for the generation of W-mode perturbations (right panel). See electronic edition of the journal for color images.

that the local stability of baroclinic perturbations in the barotropic equilibrium state is defined by the Schwarzschild-Ledoux criterion.

We study the shear flow induced linear coupling and the related possibility of the energy transfer between the different modes of perturbations using qualitative and a more detailed numerical analysis. We employ a three-mode formalism and describe the behavior of S W and P-modes under the action of the baroclinic and velocity shear forces in local approximation.

We find that the system exhibits an asymmetric coupling pattern with five energy exchange channels between three different modes. The W-mode is coupled to S and P-modes: perturbations of the potential vorticity are able to excite entropy and compressible modes. The amplitude of the generated S-mode grows with the increase of entropy stratification scale of the background ( $k_S$ ) while the amplitude of the generated P-mode perturbations grows with the increase of background baroclinic index ( $\eta$ ). The S-mode is coupled to the W and P-modes: the amplitude of the generated P-mode perturbations grows with increase of the background pressure stratification scale ( $k_P$ ), while the amplitude of the W-mode grows with the increase of baroclinic index. The P-mode is coupled to the S-mode: the amplitude of generated entropy perturbations grows with the increase of the background entropy stratification scale. On the other hand, there is no direct energy exchange channel from P to W mode and, therefore, no direct conversion is possible. Our results, however, show that the P-mode is still able



to generate W-mode through indirect three mode P-S-W coupling scheme. This linear inviscid mechanism indicates that compressible perturbations are able to generate potential vorticity via aperiodic entropy perturbations.

The dynamics of radially stratified discs have been already studied by both, linear shearing sheet formalism and direct numerical simulations. However, previous studies focus on the baroclinic stability and vortex production by entropy perturbations, neglecting the coupling with higher frequency density waves.

The most vivid signature of density wave excitation in radially stratified disc flows can be seen in Klahr (2004). The numerical results presented on the linear dynamics of perturbation SFH show high frequency oscillations after the radial wavenumber changes sign. However, focusing on the energy dynamics, the author filters out high frequency oscillations from the analysis.

The purpose of numerical simulations by Johnson and Gammie (2006) was the investigation of the velocity shear effects on the radial convective stability and the possibility of the development of baroclinic instability. Therefore, no significant amount of compressible perturbations is present initially, and it is hard to judge if high frequency oscillations appear later in simulations. Petersen et al. (2007a), (2007b) employed the anelastic approximation that does not resolve the coupling of potential vorticity and entropy with density waves. Moreover, if produced, high frequency density waves soon develop into spiral shocks (see e.g., Bodo et al 2007). The anelastic gas approximation does intentionally neglect this complication and simplifies the description down to low frequency dynamics.

Numerical simulations of hydrodynamic turbulence in unstratified disc flows showed that the dominant part of turbulent energy is accumulated into the high frequency compressional waves (see, e.g., Shen et al. 2006). On the other hand, it is vortices that are thought to play a key role in hydrodynamic turbulence in accretion discs, as well as planet formation in protoplanetary disc dynamics. Therefore, any link and possible energy exchange between high frequency compressible oscillations and aperiodic vortices can be an important factor in the above described astrophysical situations.

Based on the present findings we speculate that density waves can participate in the process of the development of regular vortical structures in discs with negative radial entropy gradients. Numerical simulations have shown that thermal (entropy) perturbations can generate vortices in baroclinic disc flows (see e.g., Petersen et al. 2007a, 2007b). Hence, vortex development through this mechanism depends on the existence of initial regular entropy perturbations, i.e., thermal plumes, in differentially rotating baroclinic disc flows.

It seems that compressional waves with linear amplitudes can heat the flow through two different channels: viscous dissipation and shear flow induced mode conversion. However, there is a strict difference between the entropy production by the kinematic shear mechanism and viscous dissipation. In the latter case, compressional waves first need to be tightly stretched down to the dissipation length-scales by the background differential rotation to be subject of viscous dumping. As a result, the entropy produced by viscous dissipation of compressional waves takes a shape of narrow stretched lines. This thermal perturbations can baroclinically produce potential vorticity of similar configuration. However, this is clearly not an optimal form of potential vorticity that can lead to the development of the long-lived vortical structures. On the contrary, entropy perturbations produced through the mode conversion channel can have a form of a localized thermal plumes. These can be very similar to those used in numerical simulations by Petersen

et al. (2007a), (2007b). In this case compressional waves can eventually lead to the development of persistent vortical structures of different polarity. Hence, high frequency oscillations of the P mode can participate in the generation of anticyclonic vortices that further accelerate dust trapping and planetesimal formation in protoplanetary discs with equilibrium entropy decreasing radially outwards.

Using the local linear approximation we have shown the possibility of the potential vorticity generation in flows with both, positive and negative radial entropy gradients (Richardson numbers). In fact, the standard alpha description of the accretion discs implies *positive* radial stratification of entropy and hence, weak baroclinic decay of existing vortices. In this case there will be a competition between the “baroclinic viscosity” and potential vorticity generation due to mode conversion. Hence, it is not strictly overruled that a significant amount of compressional perturbations can lead to the development of anticyclonic vortices even in flows with positive entropy gradients. In this case, radial stratification opens an additional degree of freedom for velocity shear induced mode conversion to operate. Although, the viability of this scenario needs further investigation.

This paper presents the results obtained within the linear shearing sheet approximation. At nonlinear amplitudes, the P mode leads to the development of shock waves. These shocks induce local heating in the flow. Therefore, a realistic picture of entropy production and vortex development in radially stratified discs with significant amount of compressible perturbations needs to be analyzed by direct numerical simulations.

## ACKNOWLEDGMENTS

A.G.T. was supported by GNSF/PRES-07/153. A.G.T. would like to acknowledge the hospitality of Osservatorio Astronomico di Torino. This work is supported in part by ISTC grant G-1217.

## REFERENCES

- Barranco, J. A., and Marcus, P. S., 2005, *ApJ* **623**, 1157  
 Bodo G., Chagelishvili G. D., Murante G., Tevzadze A. G., Rossi P. and Ferrari A., 2005, *A&A* **437**, 9  
 Bodo G., Tevzadze A. G., Chagelishvili G. D., Mignone A., Rossi, P. and Ferrari A., 2007, *A&A* **475**, 51  
 Brandenburg, A., and Dintrans, B., 2006, *A&A* **450**, 437  
 Chagelishvili G. D., Tevzadze A. G., Bodo G. and Moiseev, S. S., 1997, *Phys. Rev. Letters* **79**, 3178.  
 Fromang, S., Terquem, C., and Balbus, S. 2002 *MNRAS* **329** 18  
 Gammie, C. F. and Menou, K., 1998, *ApJ* **492**, 75  
 Goldreich P. and Lynden-Bell D., 1965, *MNRAS* **130**, 125  
 Goldreich P. and Tremaine S., 1978, *ApJ* **222**, 850  
 Heinemann, T. and Papaloizou, J. C. B. 2009a, *MNRAS* **397**, 52  
 Heinemann, T. and Papaloizou, J. C. B. 2009b, *MNRAS* **397**, 64  
 Johnson B. M. and Gammie C. F., 2005a, *ApJ* **626**, 978  
 Johnson B. M. and Gammie C. F., 2005b, *ApJ* **635**, 149  
 Johnson B. M. and Gammie C. F., 2006, *ApJ* **636**, 63  
 Isella, A., Testi, L., Natta, A., Neri, R., Wilner, D., and Qi, C., 2007, *A&A* **469**, 213  
 Klahr H. H. and Bodenheimer P., 2003, *ApJ* **582**, 869  
 Klahr H., 2004, *ApJ* **606**, 1070  
 Lerche, I. and Parker, E. N., 1967, *ApJ* **149**, 559  
 Li H., Finn J. M., Lovelace R. V. E. and Colgate S. A., 2000, *ApJ* **533**, 1023  
 Lord Kelvin (W. Tompson), 1887, *Philos. Mag.* **24**, 188  
 Lovelace R. V. E., Li H., Colgate S. A. and Nelson A. F., 1999, *ApJ* **513**, 805  
 Mamatsashvili, G. M., and Chagelishvili, G. D., 2007, *MNRAS* **381**, 809

- Petersen M. K., Julien K. and Stewart G. R., 2007a, *ApJ* **658**, 1236  
 Petersen M. K., Stewart G. R. and Julien K., 2007b, *ApJ* **658**, 1252  
 Sandin, C., Schönberner, D., Roth, M., Steffen, M., Böhm, P., and Monreal-Ibero, A. 2008, *A&A* **486**, 545  
 Sano, T., Miyama, S., Umebayashi, T., Nakano, T., 2000, *ApJ* **543**, 486  
 Shen, Y., Stone, J. M., and Gardiner, T. A., 2006, *ApJ* **653**, 513  
 Tevzadze A. G., Chagelishvili G. D., Zahn J.-P., Chanishvili R. G. and Lominadze J. G., 2003, *A&A* **407**, 779  
 Tevzadze A. G., Chagelishvili G. D. and Zahn J.-P., 2008, *A&A* **478**, 9  
 Trefethen, L. N., Trefethen, A. E., Reddy, S. C., and Driscoll, T. A., 1993, *Science* **261**, 578.  
 Volponi, F., and Yoshida, Z., 2002, *J. Phys. Soc. Japan* **71**, 1870

## APPENDIX A: INITIAL CONDITIONS

Here we present the approximations used to derive the analytic form of the initial conditions corresponding to individual modes in radially stratified shear flows. These conditions are used to construct the initial values of perturbations in the numerical integration of the ODEs governing the linear dynamics of perturbations in these flows. We employ different methods for high and low frequency modes.

### A1 P-mode

P-mode perturbations are intrinsically high frequency and well separated from low frequency modes everywhere outside the coupling region  $k_x/k_y < 1$ . In order to construct P-mode perturbations we use convective eigenfunction derived in the shearless limit and account for shear flow effects only in the adiabatic limit:

$$\Psi_c(t) = (\omega_c^2(t) + c_s^2\eta)P(t) - 2\Omega_0 W(t) - c_s^2 k_P k_x(t)s(t), \quad (\text{A1})$$

where

$$\omega_c^2(t) = -\frac{c_s^2\eta k_y^2}{c_s^2 k^2(t) - 4B\Omega_0}. \quad (\text{A2})$$

Although this form of the eigenfunction is not valid function for describing W and S modes individually in a sheared medium, it has proved to be a good tool for excluding both modes from the initial spectrum:

$$\Psi_c(0) = 0. \quad (\text{A3})$$

Assuming that we are looking for P-mode perturbations with wave-numbers satisfying the condition  $k_x(0)/k_y \gg 1$  we may use the zero potential vorticity condition:

$$W(0) = 0. \quad (\text{A4})$$

Hence, Eqs. (A3,A4) yield the full set of initial conditions for the high frequency P-mode SFH of perturbations:

$$p(0) = P_0, \quad u_x(0) = U_0, \quad (\text{A5})$$

$$u_y(0) = \frac{1}{k_x(0)}(k_y U_0 + 2BP_0), \quad (\text{A6})$$

$$s(0) = \frac{\omega_c^2(0) + c_s^2\eta}{c_s^2 k_P k_x(0)} P_0, \quad (\text{A7})$$

where  $P_0$  and  $U_0$  are free parameters corresponding to the two P-modes in the system. Specific values of these two parameters define whether the potential or kinetic part of the wave harmonic is present initially.

### A2 Low frequency modes

In order to derive the initial conditions for the S and W modes individually we employ the second order equation for radial velocity perturbation that can be derived from Eqs. (34-37):

$$\left\{ \frac{d^2}{dt^2} + c_s^2 k^2 - 4B\Omega_0 - c_s^2 \eta \right\} u_x = -c_s^2 k_y W + 4Ac_s^2 k_y p. \quad (\text{A8})$$

$$\left\{ \frac{d^2}{dt^2} + c_s^2 k^2 - 4B\Omega_0 \right\} u_y = c_s^2 k_x(t)W + 2Bc_s^2 k_P s, \quad (\text{A9})$$

For low frequency perturbations

$$\frac{d^2}{dt^2} \begin{pmatrix} u_x \\ u_y \end{pmatrix} \sim \omega_c^2 \begin{pmatrix} u_x \\ u_y \end{pmatrix}. \quad (\text{A10})$$

Assuming that  $\omega_c^2(0) \ll c_s^2 k^2(0)$  and neglecting the corresponding terms in Eqs. (A6-A7) leads to the following algebraic system:

$$[c_s^2 k^2 - 4B\Omega_0] u_x = -c_s^2 k_y W + 4Ac_s^2 k_y p. \quad (\text{A11})$$

$$[c_s^2 k^2 - 4B\Omega_0] u_y = c_s^2 k_x(t)W + 2Bc_s^2 k_P s. \quad (\text{A12})$$

Hence, we can derive the initial conditions for the low frequency modes as follows:

$$p(0) = \frac{B}{2Ac_s^2 k_y^2 + B\omega_p^2(0)} (2\Omega_0 W_0 + c_s^2 k_P k_x(0)S_0), \quad (\text{A13})$$

$$u_x(0) = \frac{1}{\omega_p^2(0)} (-c_s^2 k_y W_0 + 4Ac_s^2 k_y p(0)), \quad (\text{A14})$$

$$u_y(0) = \frac{1}{\omega_p^2(0)} (c_s^2 k_x(0)W_0 + 2Bc_s^2 k_P S_0), \quad (\text{A15})$$

where

$$\omega_p^2(0) = c_s^2 (k_x^2(0) + k_y^2) - 4B\Omega_0. \quad (\text{A16})$$

Eqs. (A11-A14) give the initial values of perturbation SFHs for S-mode when

$$W_0 = 0, \quad S_0 \neq 0, \quad (\text{A17})$$

and W-mode when

$$W_0 \neq 0, \quad S_0 = 0. \quad (\text{A18})$$